Rapid Detection of Aβ Aggregation and Inhibition by Dual Functions of Gold Nanoplasmic Particles: Catalytic Activator and Optical Reporter

Inhee Choi and Luke P. Lee*

Berkeley Sensor and Actuator Center, Department of Bioengineering, Department of Electrical Engineering and Computer Science, University of California at Berkeley, Berkeley, California 94720, United States

ABSTRACT One of the primary pathological hallmarks of Alzheimer's diseases (AD) is amyloid-β (Aβ) aggregation and its extracellular accumulation. However, current *in vitro* Aβ aggregation assays require time-consuming and labor-intensive steps, which delay the process of drug discovery and understanding the mechanism of Aβ induced neurotoxicity. Here, we propose a rapid detection method for studying Aβ aggregation and inhibition under an optimized acidic perturbation condition by dual functions of gold nanoplasmonic particles (GNPs): (1) catalytic activator and (2) optical reporter. Because of roles of GNPs as effective nucleation sites for fast-catalyzing Aβ aggregation and colorimetric optical reporters for tracking Aβ aggregation, we accomplished the fast aggregation assay in less than 1 min by the naked eyes. Our detection method is based on spontaneous clustering of unconjugated (unmodified) GNPs along with the aggregated Aβ network under an aggregation-promoting condition. As a proof-of-concept demonstration, we employed the acidic perturbation permitting rapid cooperative assemblies of GNPs and Aβ peptides *via* their surface charge modulation. Under the optimized acidic perturbation condition around pH 2 to 3, we characterized the concentration-dependent colorimetric responses for aggregation at physiologically relevant Aβ concentration levels (from 100 μM to 10 nM). We also demonstrated the GNP/acidic condition-based rapid inhibition assay of Aβ aggregation by using well-known binding reagents such as antibody and serum albumin. The proposed methodology can be a powerful alternative method for screening drugs for AD as well as studying molecular biophysics of protein aggregations, and further extended to explore other protein conformational diseases such as neurodegenerative disease.

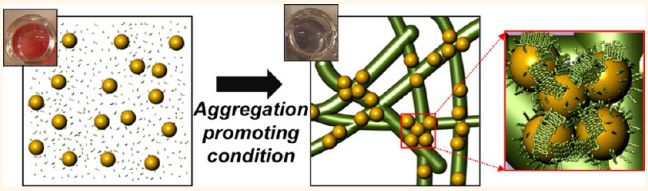

KEYWORDS: amyloid-β · Alzheimer's disease · light scattering · drug screening · nanoplasmonics · nanoparticle · nucleation · colorimetric

Alzheimer's disease (AD) is a progressive neurodegenerative disease and the leading cause of dementia in the aging population. One of the primary pathological hallmarks of AD is the formation of neutric plaques in the brain, and the aggregation (*i.e.*, oligomerization and fibrillization) of amyloid-β peptide (Aβ) is central to the formation of these plaques.[1−7] Consequently, the development of efficient methods to observe the structural evolution of Aβ from monomeric forms to oligomers and large fibrillar aggregates could provide a clue to unveil the conformational dynamics of aggregation as well as a definitive molecular basis for understanding the disease mechanism and diagnosing AD. At present, the characterization of protein structures has been commonly carried out through circular dichroism (CD) spectroscopy,[2] nuclear magnetic resonance (NMR) spectroscopy,[3,4] and X-ray crystallography.[5] Fluorescence spectroscopy combined with molecularly specific dyes (*e.g.*, thioflavin T[3,6] and Congo red[7]) has also been used to probe the formation of amyloid fibril structures. Although these methods are quite functional, most of conventional methods require complicated instrumentation, large sample volume, sample pretreatment steps (*e.g.*, precrystallization and fluorescence labeling), and long incubation (or operation) time.

As an alternative way, the observation of light scattering from gold nanoplasmonic particles can be an efficient method to monitor the dynamics of biological events and its mechanism, due to their biocompatibility,

* Address correspondence to lplee@berkeley.edu.

Received for review May 7, 2013 and accepted June 18, 2013.

Published online June 18, 2013
10.1021/nn402310c

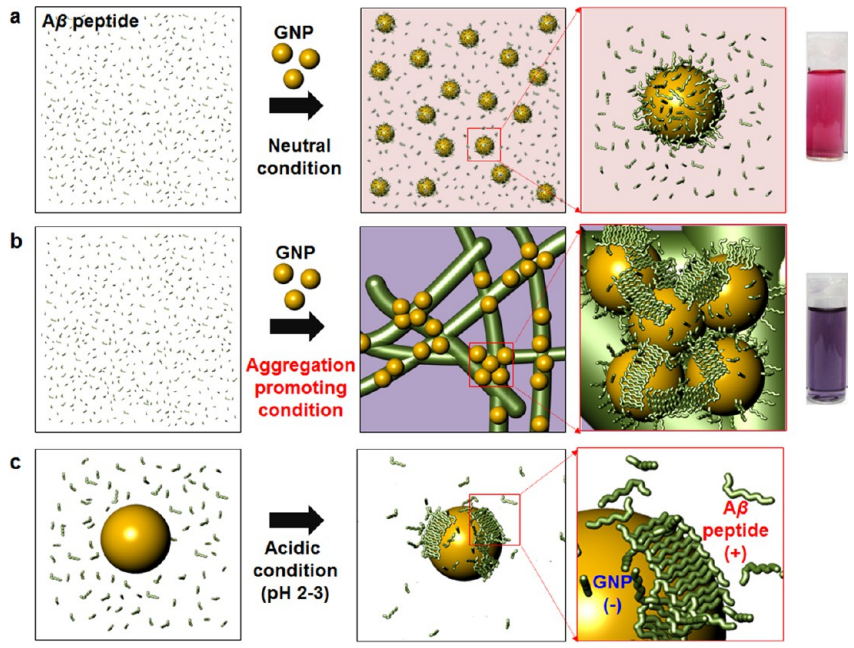

Figure 1. Schematic illustrations of the dual functions of gold nanoplasmonic particle (GNP) associated Aβ aggregation and its colorimetric detection. (a) Under a neutral condition (*e.g.*, pH 7.4 buffer condition), GNP can provide a nucleation site for further Aβ aggregation. (b) Under an aggregation-promoting condition (*e.g.*, acidic condition), GNPs promptly assemble with Aβ peptides, which results in strong plasmon coupling along with the aggregated network. Collectively, GNP acts as a catalytic core and a colorimetric reporter for tracking the molecular assembly of Aβ peptides. (c) Description of the interaction between the Aβ peptides and the GNPs under the acidic condition: it is likely to be dominated by an electrostatic interaction between positively charged Aβ and negatively charged GNPs at pH 2−3.

photostability, and superior optical properties such as an enhanced scattering property.[8,9] In this regard, the conjugation of biomolecules on plasmonic nanoparticles may offer many new opportunities to develop diagnostic methods, therapeutics, and medicines.[9−12] Considering that *in vivo* protein aggregation usually takes place at interface like cellular membrane, gold nanoparticle also offers a desirable interface for studying protein molecular assembly by controlling its surface property (*e.g.*, surface charge and hydrophobicity). Recent reports demonstrated that protein conjugated gold nanoplasmonic particles can be utilized as an excellent colorimetric reporter for tracking the structural evolution under protein destabilizing conditions[13] as well as diagnosing the progress of the protein aggregation at each sampling point.[14] Likewise, the behavior of the protein-conjugated nanoparticles could be further extended to examine the molecular assembly of other small biomolecules (*e.g.*, peptides), which have critical implications for diseases.

In particular, Yokoyama *et al.* systemically studied the conjugation of Aβ peptides on gold colloidal nanoparticles by varying the nanoparticles size,[15] pH value,[16] and temperature.[17] They reported the reversibility of the conjugation of Aβ peptides onto the gold colloidal nanoparticles. Wang *et al.* presented that the complex structures composed by streptavidin conjugated gold nanoparticles and biotin modified Aβ peptides are able to detect different sequence of Aβ peptides *via* the disassembly induced by differential affinity to Zn(II) ion of two peptide sequences.[18] Han *et al.* successfully demonstrated that the conjugation of Aβ peptides to the gold nanoparticle *via* biotin−streptavidin interaction is also applicable to screen an aggregation inhibitor through the long time incubation (48 h) under a neutral condition (pH = 7.2).[19] Sakono *et al.* showed that Aβ antibody conjugated gold nanoparticles allows to detect matured Aβ aggregates within 1 h.[20] It is noteworthy that these recent results related with Aβ would pave a new way to study protein aggregation and diagnose protein conformational diseases. However, the catalytic function of the gold nanoplasmonic particle in itself during the biomolecular assemblies (*e.g.*, peptide or protein aggregation) has been overlooked in these previous studies.

During the nanoparticle associated biomolecular assembly, the interactions between nanoparticles and biomolecules can vary from covalent interactions to noncovalent interactions (*e.g.*, hydrogen bonding, electrostatic interactions, hydrophobic, and van der Waals force). Owing to these interactions, colloidal gold nanoparticles can act as nucleation sites for biomolecular self-assembly because Brownian motion of the nanoparticles increases the number of collisions between nanoparticles and molecules.[21,22] As a result, gold nanoparticles could be used to promote the biomolecular self-assembly (*i.e.*, oligomerization and fibrillization) as seeds and to permit rapid monitoring of the aggregation propensity through a seeded polymerization process,[23] compared to the case of their absence. Until now, we note that it usually takes a long incubation time to investigate the

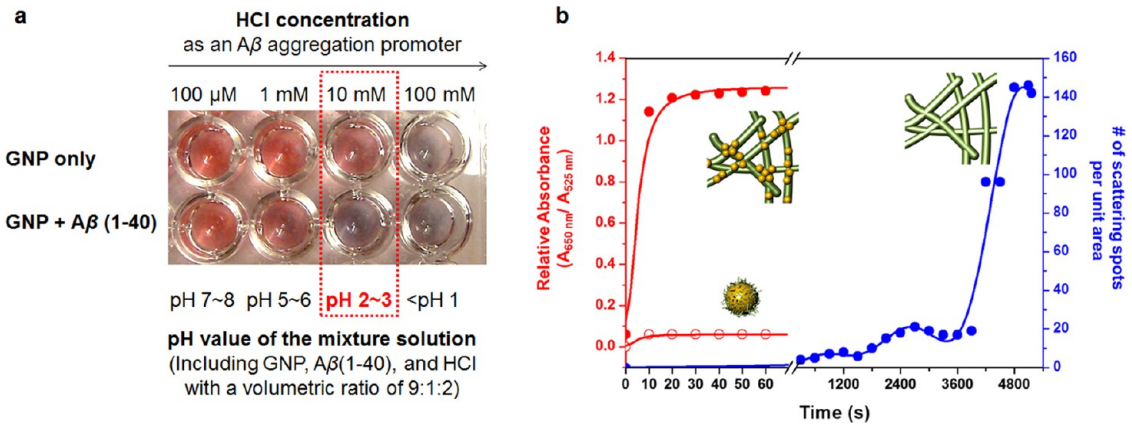

Figure 2. Determination of an optimal acidic perturbation condition and comparison of Aβ aggregation kinetics according to the incubation conditions. (a) Determination of a perturbation condition (*i.e.*, pH level) for ultrafast assemblies of Aβ monomers without a self-aggregation of GNPs. (b) Comparison of Aβ aggregation kinetics according to the incubation conditions. (Closed red circles, left axis) The change in the relative absorbance of the 100 μM Aβ (1−40) solution incubated with GNPs under an acidic condition (pH 2−3). (Open red circles, left axis) The change in the relative absorbance of the 100 μM Aβ (1−40) solution incubated with GNPs under a neutral condition (pH 7.4). (Closed blue circles, right axis) The increase in the number of scattering spots counted from the time-resolved dark−field images (see also snapshots in Supplementary Figure S2) of the 100 μM Aβ (1−40) solution incubated without GNPs under the acidic condition (pH 2−3).

Aβ aggregation propensity by using the conventional techniques,[2−7] since (1) the fibrillization is a slow process (see Supplementary Table S1) and (2) the assays are usually performed through separately sampling and sequential measuring. On the contrary, the molecularly driven dynamic change in the interparticle distance of gold nanoparticles during biomolecular assembly can be readily detected by the naked eyes owing to the distance dependent optical scattering of nanoplasmonic particles. Consequently, gold nanoparticles allow *in situ* colorimetric assay for detecting dynamic biomolecular assembly without sampling and further pretreatment steps.

Herein, we demonstrate a facile, rapid, plasmonic detection method to track Aβ aggregation (molecular assembly) propensity and its inhibition. Our method is based on a spontaneous clustering of unmodified gold nanoplasmonic particles (GNPs) along with the Aβ fibril-like network under intentional perturbation conditions, which can be easily read out without instrumentation. In our proposed method, the advantage of using a GNP is twofold: (1) it rapidly catalyzes Aβ aggregation, and (2) it allows simple colorimetric detection for Aβ aggregation with the naked eyes. Since GNPs can act as nucleation sites for Aβ aggregation (Figure 1a), we expected that both Aβ monomers and GNPs in aqueous suspension would promptly assemble into the largely aggregated network when they are exposed to aggregation-promoting conditions [*i.e.*, GNP (seed) + excessive Aβ monomers → GNP/Aβ*s* (nuclei) + remaining Aβ monomers → GNP/Aβ*s* (large aggregate)]. The subsequent changes in the dynamic distance between the GNPs (Figure 1b) enable GNPs to function as colorimetric reporters for Aβ molecular assembly *via* plasmon coupling between the GNPs in the assembled network (*e.g.*, when dimers are formed, $\Delta\lambda_{PR}(x) = A\ e^{-x/D}$, where λ_{PR} is the plasmon resonance peak wavelength, x is interparticle distance, and A and D are constant).[24] Consequently, we can rapidly detect color changes induced by the molecular assembly of Aβ with varying the perturbation conditions (*e.g.*, pH, temperature, and chemical additives). By observing the rapid color change of GNPs solution, we can also readily elucidate Aβ aggregation kinetics and examine its inhibitor as a possible therapeutic reagent. As a proof-of-concept demonstration, we employed acidic perturbation permitting rapid cooperative assemblies of GNPs and Aβ peptides *via* their surface charge modulation (GNP$^{(-)}$ + A$\beta^{(+)}$ → GNP/Aβ, Figure 1c). It should be noted that the interaction between the Aβ peptides and the GNPs surface is most likely to be dominated by an electrostatic interaction between positively charged Aβ ($\because$ pI of A$\beta \approx$ pH 5.5 > pH 2−3)[25] and negatively charged GNP surface (due to citrate moieties) at pH 2−3. We describe below a series of proof-of-concept experiments.

RESULTS AND DISCUSSION

The employed methodology is illustrated in Figure 1. Our technique has several key advantages: it is simple and fast as it involves mixing Aβ peptides with an aqueous GNP solution, adding reagents (*i.e.*, aggregation-promoters and/or inhibitors), observing the clearly visible color change of the mixture solution by the naked eyes. In our typical experiment, unmodified GNPs stabilized by citrate moieties (20 nm in diameter, *ca.* 1 nM) were mixed with Aβ (1−40) monomers of physiologically relevant micromolar concentration at an optimal ratio (9:1 v/v), where the number of Aβ (1−40) monomers is extremely larger than that of GNPs (*e.g.*, 4 orders of magnitude larger at 100 μM Aβ monomer). And then we dropwisely added hydrochloric acid (HCl), as an aggregation promoter, into the prepared mixture solution since low pH condition

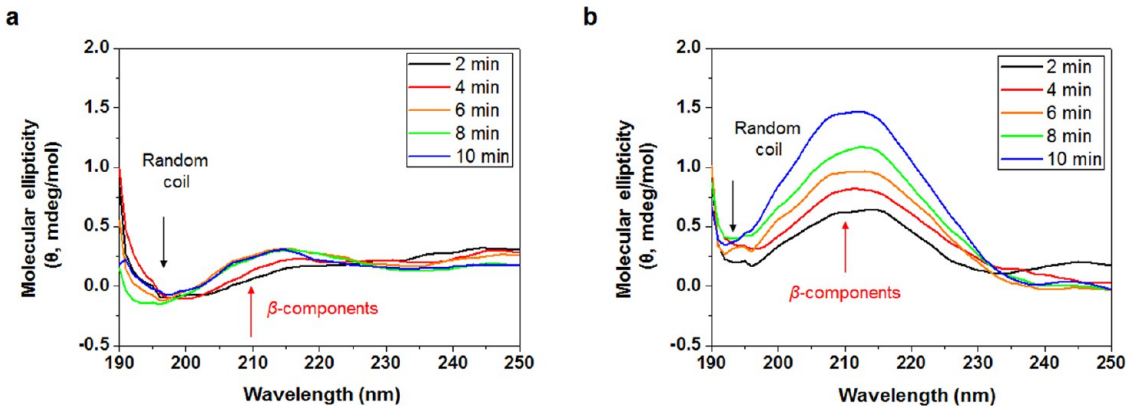

Figure 3. Circular dichroism spectra for both cases of absence and presence of GNPs during Aβ aggregation. (a) 100 μM Aβ (1−40) incubated without GNPs under acidic condition: a random coil-related band was dominantly observed, which is attributable to the formation of disordered and partially unfolded Aβ species (*e.g.*, monomeric or oligomeric) under acidic condition. And a β-components (*i.e.*, β-sheet and β-turn)-related band, derived from fibrillar aggregation, was slowly increased with increasing time. (b) The 100 μM Aβ (1−40) incubated without GNPs under acidic condition: the β-components-related band was significantly increased with increasing time, while decreasing the random coil-related band.

is well-known as an aggregation-promoting condition for Aβ.[26−28] By varying the concentration (from 100 μM to 100 mM) of HCl, we determined the optimal acidic perturbation condition where a self-aggregation of GNPs due to the high ionic strength of medium is prohibited. After dropwisely adding a low concentration of HCl (100 μM), no significant changes were observed for both an Aβ (1−40) + GNP mixture solution and a GNP solution (Figure 2a). Addition of 1 mM HCl induced slight color change of the GNP solution in the presence of Aβ (1−40) monomers, whereas no color change was observed in the absence of Aβ (1−40) monomers. When we added 10 mM HCl to the mixture of Aβ (1−40) monomers and GNPs (note: pH value of the resulting Aβ (1−40) + GNP mixture solution was around pH 2−3), we observed a dramatic color change from red to violet within only 20 s, whereas a minor color change was observed in the absence of Aβ monomers (*i.e.*, GNPs only) (Figure 2a). Likewise, time-resolved dark-field scattering images of the mixed solution under an identical perturbation condition show dramatic changes in the scattering color of the assembled GNPs in the presence of Aβ monomers (Supplementary Figure S1). This can be attributed to the ultrafast clustering of GNPs along with the Aβ network assembled under the given acidic condition. However, a high concentration of HCl (100 mM, below pH 1) also induces the self-aggregation of GNPs so that it is difficult to distinguish the self-aggregation of GNPs from clustering of GNPs along with the aggregation network of Aβ. On the basis of these results, we selected the condition of pH 2−3 induced by dropwise addition of 10 mM HCl, as a perturbation condition for a proof-of-concept demonstration of the proposed method.

Figure 2b shows a dramatic (within 20 s) change in a relative absorbance for two distinct peaks involved in the assemblies of 100 μM Aβ incubated with GNPs under the predetermined acidic condition (closed red circles). On the contrary, no significant change was observed in the Aβ solution incubated under neutral condition with GNPs within the short time range (open red circles). In the case of an absence of the GNPs, we observed white scattering spots (in dark-field images of Supplementary Figure S2) induced by light scattering of Aβ aggregates formed after longer incubation (*ca.* 1 h) than that of a presence of GNPs under the identical acidic perturbation condition (around pH 2−3, see closed blue circles in Figure 2b).

To characterize the structural transition during Aβ aggregation, circular dichroism (CD) spectra were obtained for both cases of absence and presence of GNPs during Aβ incubation under acidic condition. Results show that similar transitions of random coil to β-components abundant structures in time-resolved CD spectra for both cases supporting the nanoparticle-mediated aggregation are not fundamentally different from those that occur physiologically (Figure 3). However, the remarkable difference in aggregation kinetics was observed as we intentionally induced Aβ aggregation for the fast detection. In detail, in the case of Aβ incubated without GNPs under acidic condition, a random coil-related band was dominantly observed, which is attributable to the formation of disordered and partially unfolded Aβ species (*e.g.*, monomeric or oligomeric) under acidic condition. And a β-components (*i.e.*, β-sheet and β-turn)-related band, derived from fibrillar aggregation, was slowly increased with increasing time (Figure 3a). On the other hand, when we incubated Aβ monomers with GNPs under acidic condition, the β-components-related band was significantly increased with increasing time, while decreasing the random coil-related band (Figure 3b). We would like to note that the conversion of random coil to β-component abundant structures during Aβ aggregation is generally accepted.[29] The observed drastic spectral increase of the β-components-related band

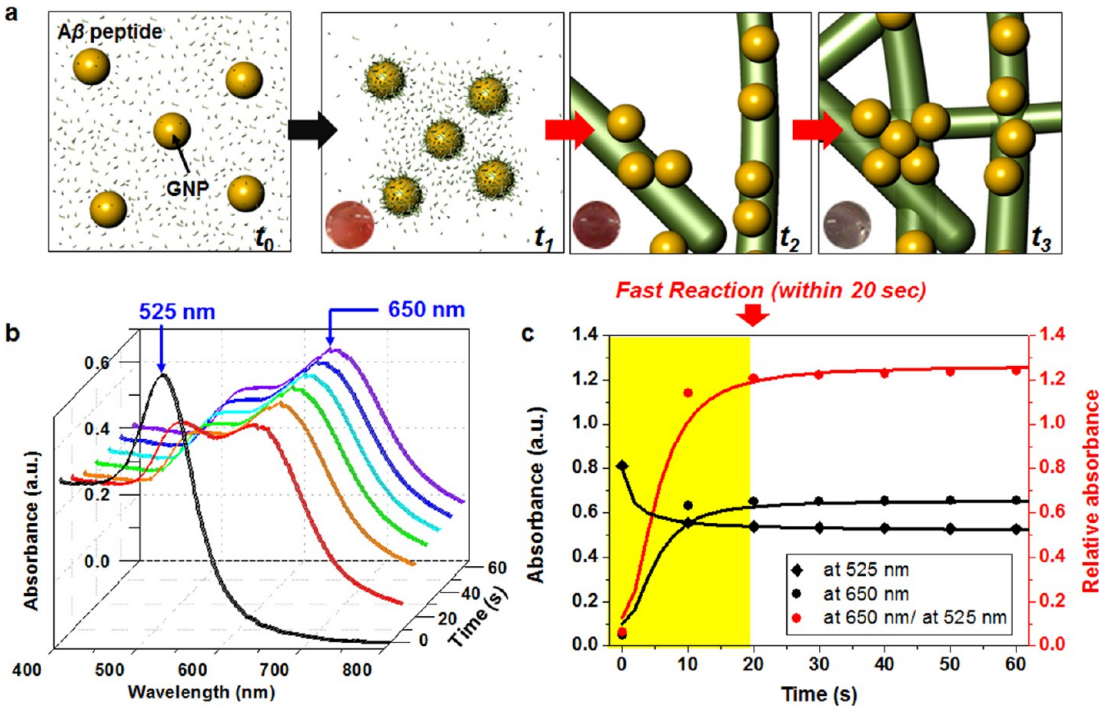

Figure 4. Time-resolved observation of GNP catalyzed rapid Aβ aggregation under the acidic perturbation condition. (a) A schematic illustration for a time-lapse behavior of GNPs associated with Aβ peptides under the acidic condition. Insets show representative colors of the mixture solution in accordance with the progress of Aβ aggregation. (b) A representative time-resolved spectral change of the mixture solution of 20 nm GNPs and Aβ (1−40) peptides under the acidic condition. (c) A plot depicting a relative absorbance between an initial peak position (at 525 nm) and a newly formed peak position (at 650 nm) at each time frame.

when incubating with GNPs supports clearly our hypothesis of nanoparticle-catalyzed rapid Aβ aggregation. Taken together, dark-field imaging and CD analyzing results support our concept that GNP promotes molecular assembly of Aβ under the acidic condition.

To further confirm that the observed color change is due to the molecular assembly of Aβ, we also performed identical tests with varying amounts (0−50%) of 2,2,2-trifluoroethanol (TFE), which has been extensively used as a amyloid-promoting reagent.[2,30] Within 1 min after adding TFE, we also observed distinct color change from red to purple, and followed by bluish violet, which shows obvious time- and dose-dependent responses (Supplementary Figure S3). The increase of an incubation temperature also induced the color change in the mixture solution of GNPs and Aβ (1−40) peptides (Supplementary Figure S4).

Having demonstrated that the molecular assembly of Aβ under the various perturbation conditions (*i.e.*, pH levels, the amount of an additive, and temperature) can be rapidly tracked by the naked eyes in real-time, we next investigated its reaction dynamics under a given perturbation condition. For further study of Aβ aggregation, we exploited the acidic perturbation condition of pH 2−3 predetermined earlier. After a dropwise addition of the 10 mM HCl into the mixture solution of GNPs and 100 μM Aβ (1−40) peptides, we measured spectral changes *via* UV−visible spectroscopy every 10 s. Figure 4b shows a representative time-resolved spectral change of the mixture solution induced by Aβ aggregation. It is noteworthy that we typically observe not only a red-shift of the intrinsic plasmon band of 20 nm GNPs (around 525 nm), but also the decrease of its intensity and the appearance of another longer wavelength plasmon band (around 650 nm) as an indicator of longitudinal fibril-like assembly for Aβ aggregation. A plot depicting relative absorbance ratios between an initial peak position (at 525 nm) and a newly formed peak position (at 650 nm) at each time frame (Figure 4c) suggests the increase in the number of GNPs clustered along with the fibril-like networks as time passes (described in Figure 4a). Within 20 s, this ratio quickly increased and reached its maximum, with no significant change observable afterward. This rapid increase of the absorbance ratio under the acidic perturbation condition can be attributed to two factors: (1) Aβ (1−40) peptides become partially folded intermediates under an acidic condition, which are rapidly prone to undergo oligomerization and further aggregation.[26−28] and (2) GNPs provide nucleation sites for the folded Aβ peptides during the aggregation process.[31,32] In general, folding Aβ monomers is well-known as a rate-limiting step for aggregation process[28,33] and nucleation-dependent polymerization is generally accepted for explaining a fibrillization mechanism.[26−28] Once the nucleus is formed, further polymerization of Aβ peptides is accelerated (*i.e.*, monomer ⇔ partially folded intermediate ⇔ nucleus → fibril or large aggregate).

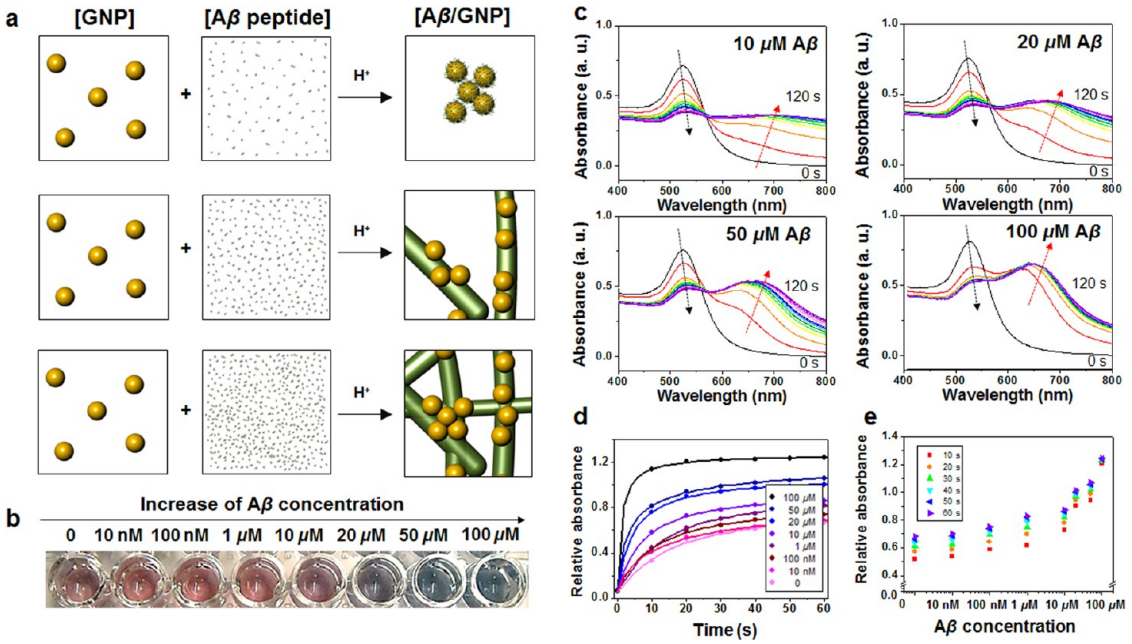

Figure 5. Plasmonic monitoring of Aβ concentration-dependent aggregation under the acidic perturbation condition. (a) Cartoons for Aβ concentration dependent association of GNPs under the acidic perturbation condition. (b) Aβ concentration dependent colorimetric responses measured from 10 nM to 100 μM. (c) Time-resolved spectral changes of the Aβ (1−40) + GNP mixture solution under the acidic perturbation condition: Each plot is for 10, 20, 50, and 100 μM Aβ (1−40), respectively. UV−visible spectra were measured every 10 s for 2 min. Arrows indicate trends in time-resolved spectral shift at each plasmon band. (d) Aβ concentration dependent kinetic profile of aggregation depicted by the changes in relative absorbance ratios ($A_{650\ nm}/A_{525\ nm}$). (e) A graph depicted for Aβ concentration *vs* relative absorbance at each time frame from 10 to 60 s.

Accordingly, we can achieve rapid monitoring of Aβ aggregation under the given acidic condition by speeding-up an assembly rate with the aid of GNPs providing a nucleation site (*i.e.*, it eliminates a long lag-time to form nucleus by Aβ monomers themselves).

We next investigated aggregation propensity at different concentrations of Aβ monomers. Aβ (1−40) monomer samples with initial concentrations ranging from 100 μM down to 10 nM (*i.e.*, physiologically relevant Aβ concentrations) were prepared and mixed with the 20 nm GNP solution, and then exposed to the predetermined identical acidic perturbation condition (Figure 5a). We hypothesized that the extent of Aβ aggregation and its resulting structural characteristics are dependent on an initial Aβ concentration.[28,34] As we expected, the solution turns from red to purple and bluish violet (Figure 5b) within 1 min, which are colors easily distinguishable at a glance. Figure 5c shows time-resolved spectral changes at each concentration of Aβ monomers. The changes in relative absorbance ratios ($A_{650\ nm}/A_{525\ nm}$) clearly show the concentration dependent sigmoidal kinetic profile of Aβ aggregation, which are used for the quantification. The most significant change during the reaction occurs within 20 s after exposure to the acidic condition (Figure 5d). The steep slope of the sigmoidal curve can be explained as an ultrafast assembly rate under the acidic condition. The remarkable difference in an initial slope is a main driving force to induce a distinguishable colorimetric response within several seconds according to the peptide concentration (Supplementary Figure S5). As a result, the concentration dependent changes in colors and spectra were distinguishable within even at 10 s, and which showed a similar trend afterward (Figure 5e). The dark-field images of the resulting solutions clearly show an increase in the sizes of the clustered GNPs dependent upon initial Aβ monomer concentrations (Supplementary Figure S6). We would like to emphasize that it is difficult to differentiate the concentration dependent Aβ aggregation propensity if we perform similar tests by using the GNPs preconjugated with Aβ monomers (Aβ/GNPs, functioning as nucleus). Irrespective of free Aβ concentration, preconjugated Aβ/GNPs are preferentially aggregated among themselves rather than being cooperatively assembled by GNPs and free Aβ monomers (Supplementary Figure S7a). This is a reason we use unconjugated (unmodified) GNP for tracking Aβ aggregation (Supplementary Figure S7b).

The data presented above supports that our method is a simple and efficient way for rapidly monitoring Aβ aggregation propensity. We further investigated antiaggregation of Aβ by adding well-known Aβ binding reagents such as human serum albumin (HSA) and anti-Aβ antibody. It is obvious that Aβ aggregation would be inhibited by pretreatment with binding reagents (Figure 6a), since their selective binding to Aβ peptide lowers the level of free Aβ monomers and oligomers at an initial growth stage. After 5 min incubation of Aβ (1−40) monomer solution (containing GNPs) with 100 μM HSA and 100 μg/mL anti-Aβ (1−40) antibody, respectively,

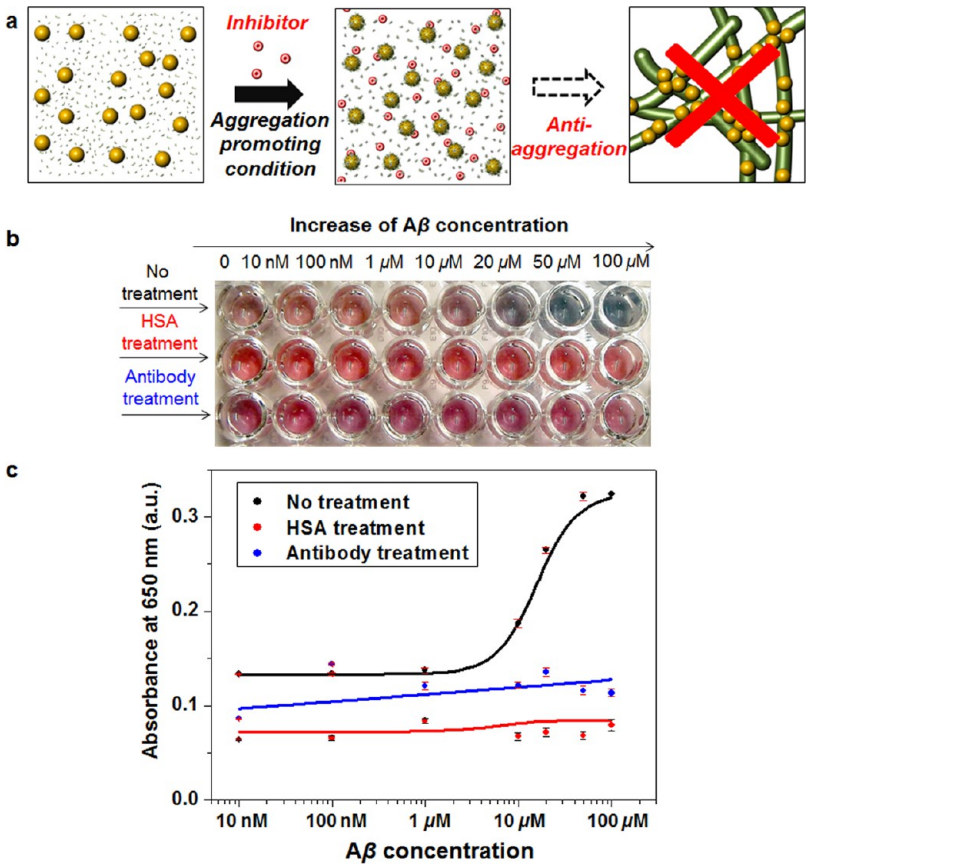

Figure 6. Inhibition of Aβ aggregation by human serum albumin (HSA) and anti-Aβ antibody. (a) A schematic illustration of the inhibition of Aβ aggregation by inhibitors. (b) Colorimetric responses of antiaggregation by treatment with binding reagents (*i.e.*, HSA and antibody). (c) The resulting changes in absorbance measured at 650 nm as an indicator of longitudinal fibril-like assembly for Aβ aggregation. Result is representative of three independent experiments. Error bars are included on all data points.

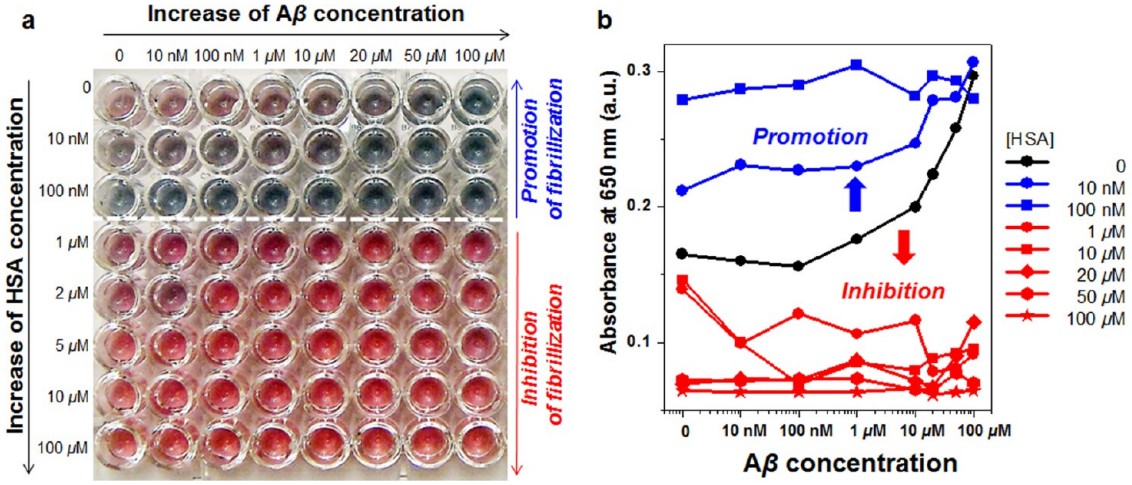

Figure 7. Plasmonic screening of dose-dependent antiaggregation effect of HSA. (a) Colorimetric responses of antiaggregation by the treatment with HSA of different concentration from 10 nM to 100 μM (b) The corresponding changes in absorbance measured at 650 nm as an indicator peak of large fibrillar aggregation.

they were exposed to the acidic condition. Figure 6b shows a minimal color change in the presence of the inhibitors (middle and lower rows), indicating clear antiaggregation effects compared with the untreated case (upper row). The treatment with anti-Aβ (1−40) antibody induced a slight red-shift; however, it maintained the color without further change for a long time. HSA also induce the almost no change of the solution. The observed colorimetric response for antiaggregation can be also corroborated by measuring the increase in absorbance measured at 650 nm with a conventional plate reader, as shown in Figure 6c. No significant increase of

the indicator peak of fibril-like assembly (at 650 nm) was observed in the Aβ monomer solutions preincubated with inhibitors. The inhibition of Aβ aggregation by serum albumin and antibody has been consistently reported through a number of studies.[35−39] This reveals that the suggested method is also efficient for studying the aggregation inhibition, and that it can be a powerful alternative way for conventional screening methods to track a protein aggregation (or inhibition) propensity.

Moreover, this result provides a facile method for drug screening of AD and finding optimum dose for preventing aggregation. We further investigated antiaggregation of Aβ by adding different amount of inhibitors. We first test this concept with HSA, which is well-known as one of the component lowering the Aβ level in blood and cerebrospinal fluid (CSF) by dynamic equilibrium across the blood−brain barrier.[35,36,40] We observed the dose-dependent antiaggregation effect of HSA (Figure 7a,b and Supplementary Figure S8). This can be attributed to the decrease of the amount of the accessible Aβ monomers for the further aggregation due to the high affinity of monomeric Aβ for HSA. On the basis of our results tested under physiological micromolar Aβ concentration, the large fibrillar aggregation is successfully inhibited by the treatment with HSA of over 1 μM. Interestingly, aggregation is rather promoted at the concentration below 1 μM HSA. Considering the level of HSA in the normal CSF (3 μM) and its micromolar affinity for Aβ (K_d = 5−10 μM),[35] our observation is quite persuasive in terms of explaining the homeostasis of *in vivo* Aβ aggregation under normal physiological condition. In other words, it can be interpreted that Aβ aggregation is effectively being inhibited by HSA under normal physiological condition. Similarly, the dose-dependent antiaggregation effect by anti-Aβ antibody was also successfully demonstrated (Supplementary Figure S9).

Finally, another consideration that arises from these data relates to the design and development of drugs. Application of the proposed method to develop new platform for designing personalized medicine is currently under investigation.

CONCLUSIONS

In conclusion, we accomplished an efficient method that allows a simple, fast, real-time colorimetric monitoring of the molecular assembly of Aβ monomers under the perturbation conditions. The dual roles of GNPs in the proposed method, (1) nucleation sites and (2) colorimetric reporters, enabled us to easily detect the aggregation progress within even 20 s by the naked eyes. As a model system, we employed acidic perturbation (around pH 2−3) permitting rapid cooperative assemblies of GNPs and Aβ peptides *via* their surface charge modulation. As a result, we clearly observed concentration dependent colorimetric responses for the molecular assembly of Aβ at physiologically relevant micromolar concentrations. Moreover, we demonstrated the GNP/acidic condition-based rapid inhibition assay of Aβ aggregation by using well-known binding reagents such as antibody and serum albumin. This finding provides a facile method for drug screening of AD and determining optimum dose for preventing aggregation. Finally, we propose that this method can be extended to explore the aggregation (and/or antiaggregation) of other proteins, which induce the protein conformational disorders.

EXPERIMENTAL DETAILS

Materials. Gold nanoparticles (GNPs, 20 nm in diameter) were purchased from BBI international, INC. Amyloid β fragment 1−40 [Aβ (1−40)] were purchased from AnaSpec. Human serum albumin and 2,2,2-trifluoroethanol (TFE) were purchased from Sigma and Sigma-Aldrich, respectively. Polyclonal anti-Aβ (1−40) antibody was obtained from Invitrogen.

Plasmon Based Colorimetric Assay for Aβ Aggregation. In our typical experiment, 90 μL of GNPs (*ca.*, 1 nM) was mixed with 10 μL of Aβ (1−40) monomers at physiologically relevant concentration range (from 100 μM to 10 nM) with the optimal ratio (9:1 v/v), where the number of Aβ monomers is much larger than that of GNPs (*e.g.*, 4 orders of magnitude larger at 100 μM Aβ monomer). To induce fast molecular assembly of Aβ monomers, we intentionally added 20 μL of hydrochloric acid (HCl) into the prepared GNP + Aβ monomer mixture solution, as a proof-of-model demonstration. By varying the concentration (from 100 μM to 100 mM) of HCl, we determined the optimal perturbation condition for the assay. Similar tests were also carried out by TFE treatment, which is well-known as an amyloid forming reagent. Under the given perturbation conditions, the absorbance of solution was measured *via* UV−visible spectroscopy (for a full-wavelength range spectrum) and microplate reader (for an end-point absorbance at a specific wavelength) in order to quantify the observed color change.

Dark-Field Imaging. For the dark field imaging, an Olympus BX-51 microscope equipped with a water (oil) immersion dark-field condenser (NA = 1.2−1.4) and CCD camera (Q-COLOR3) was used. A homemade PDMS fluidic chamber was prepared to confine the mixture solution of Aβ monomers and GNPs.

Circular Dichroism Spectroscopy. The secondary structures of Aβ aggregates were characterized by Chirascan-plus CD-spectrometer (Applied Photophysics, U.K.). CD spectra were recorded from 190 to 260 nm. All CD measurements were recorded by averaging of two runs.

Colorimetric Screening of Antiaggregation of Aβ by Inhibitors. For the colorimetric screening of antiaggregation, the Aβ (1−40) monomers, GNPs, and inhibitors (*e.g.*, HSA and anti-Aβ antibody) were preincubated with for 5 min, and then exposed to the identical acidic perturbation condition. The volumetric ratio of the GNP, Aβ (1−40), inhibitor, and 10 mM HCl was set to 9:1:1:2. By varying the concentration of the inhibitors, dose-dependent colorimetric responses for antiaggregation were observed by the naked eyes and the microplate reader.

Conflict of Interest: The authors declare no competing financial interest.

Supporting Information Available: Experimental data including time-lapse dark-field images of Aβ incubated without and with GNPs under the acidic condition, optical responses under the TFE-induced and heat-induced Aβ aggregation, Aβ concentration dependent assembly rate, dark-field images of the clustered GNPs dependent on Aβ monomer concentrations, another set of plasmonic screening results for dose-dependent antiaggregation effect of HSA and colorimetric responses of dose-dependent

antiaggregation by addition of anti-Aβ antibody. This material is available free of charge *via* the Internet at http://pubs.acs.org.

Acknowledgment. This research was supported by the Converging Research Center Program funded by the Ministry of Education, Science and Technology (2012K001363) of Korea and Samsung Electronics, Inc.

REFERENCES AND NOTES

1. LaFerla, F. M.; Green, K. N.; Oddo, S. Intracellular Amyloid-Beta in Alzheimer's Disease. *Nat. Rev. Neurosci.* **2007**, *8*, 499–509.
2. Fezoui, Y.; Teplow, D. B. Kinetic Studies of Amyloid Beta-Protein Fibril Assembly—Differential Effects of Alpha-Helix Stabilization. *J. Biol. Chem.* **2002**, *277*, 36948–36954.
3. Chimon, S.; Ishii, Y. Capturing Intermediate Structures of Alzheimer's Beta-Amyloid, A beta(1−40), by Solid-State NMR Spectroscopy. *J. Am. Chem. Soc.* **2005**, *127*, 13472–13473.
4. Baldwin, A. J.; Anthony-Cahill, S. J.; Knowles, T. P. J.; Lippens, G.; Christodoulou, J.; Barker, P. D.; Dobson, C. M. Measurement of Amyloid Fibril Length Distributions by Inclusion of Rotational Motion in Solution NMR Diffusion Measurements. *Angew. Chem., Int. Ed.* **2008**, *47*, 3385–3387.
5. Inouye, H.; Fraser, P. E.; Kirschner, D. A. Structure of Beta-Crystallite Assemblies Formed by Alzheimer Beta-Amyloid Protein Analogs—Analysis by X-Ray-Diffraction. *Biophys. J.* **1993**, *64*, 502–519.
6. Meier, M.; Kennedy-Darling, J.; Choi, S. H.; Norstrom, E. M.; Sisodia, S. S.; Ismagilov, R. F. Plug-based Microfluidics with Defined Surface Chemistry to Miniaturize and Control Aggregation of Amyloidogenic Peptides. *Angew. Chem., Int. Ed.* **2009**, *48*, 1487–1489.
7. Miura, T.; Yamamiya, C.; Sasaki, M.; Suzuki, K.; Takeuchi, H. Binding Mode of Congo Red to Alzheimer's Amyloid Beta-Peptide Studied by UV Raman Spectroscopy. *J. Raman Spectrosc.* **2002**, *33*, 530–535.
8. Ghosh, S. K.; Pal, T. Interparticle Coupling Effect on the Surface Plasmon Resonance of Gold Nanoparticles: From Theory to Applications. *Chem. Rev.* **2007**, *107*, 4797–862.
9. Dykman, L.; Khlebtsov, N. Gold Nanoparticles in Biomedical Applications: Recent Advances and Perspectives. *Chem. Soc. Rev.* **2012**, *41*, 2256–2282.
10. Aili, D.; Stevens, M. M. Bioresponsive Peptide-Inorganic Hybrid Nanomaterials. *Chem. Soc. Rev.* **2010**, *39*, 3358–70.
11. Lu, Y.; Liu, J. W. Smart Nanomaterials Inspired by Biology: Dynamic Assembly of Error-Free Nanomaterials in Response to Multiple Chemical and Biological Stimuli. *Acc. Chem. Res.* **2007**, *40*, 315–323.
12. Liu, J. W.; Lu, Y. Smart Nanomaterials Responsive to Multiple Chemical Stimuli with Controllable Cooperativity. *Adv. Mater.* **2006**, *18*, 1667–1671.
13. Choi, I.; Yang, Y. I.; Jeong, E.; Kim, K.; Hong, S.; Kang, T.; Yi, J. Colorimetric Tracking of Protein Structural Evolution Based on the Distance-Dependent Light Scattering of Embedded Gold Nanoparticles. *Chem. Commun.* **2012**, *48*, 2286–2288.
14. Hong, S.; Choi, I.; Lee, S.; Yang, Y. I.; Kang, T.; Yi, J. Sensitive and Colorimetric Detection of the Structural Evolution of Superoxide Dismutase with Gold Nanoparticles. *Anal. Chem.* **2009**, *81*, 1378–1382.
15. Yokoyama, K.; Briglio, N. M.; Hartati, D. S.; Tsang, S. M. W.; MacCormac, J. E.; Welchons, D. R. Nanoscale Size Dependence in the Conjugation of Amyloid Beta and Ovalbumin Proteins on the Surface of Gold Colloidal Particles. *Nanotechnology* **2008**, *19*, 375101.
16. Yokoyama, K.; Welchons, D. R. The Conjugation of Amyloid Beta Protein on the Gold Colloidal Nanoparticles' Surfaces. *Nanotechnology* **2007**, *18*, 105101.
17. Yokoyama, K.; Gaulin, N. B.; Cho, H.; Briglio, N. M. Temperature Dependence of Conjugation of Amyloid Beta Protein on the Surfaces of Gold Colloidal Nanoparticles. *J. Phys. Chem. A* **2010**, *114*, 1521–1528.
18. Wang, C. K.; Liu, D. J.; Wang, Z. X. Resonance Light Scattering as a Powerful Tool for Sensitive Detection of Beta-Amyloid Peptide by Gold Nanoparticle Probes. *Chem Commun* **2011**, *47*, 9339–9341.
19. Han, S. H.; Chang, Y. J.; Jung, E. S.; Kim, J. W.; Na, D. L.; Mook-Jung, I. Effective Screen for Amyloid Beta Aggregation Inhibitor Using Amyloid Beta-conjugated Gold Nanoparticles. *Int. J. Nanomed.* **2011**, *6*, 1–12.
20. Sakono, M.; Zako, T.; Maeda, M. Naked-eye Detection of Amyloid Aggregates Using Gold Nanoparticles Modified with Amyloid Beta Antibody. *Anal. Sci.* **2012**, *28*, 73–76.
21. Glotzer, S. C.; Solomon, M. J.; Kotov, N. A. Self-Assembly: From Nanoscale to Microscale Colloids. *AIChE J.* **2004**, *50*, 2978–2985.
22. Wang, T.; Lamontagne, D.; Lynch, J.; Zhuang, J.; Cao, Y. C. Colloidal Superparticles from Nanoparticle Assembly. *Chem. Soc. Rev.* **2013**, *42*, 2804–23.
23. Alvarez-Martinez, M. T.; Fontes, P.; Zomosa-Signoret, V.; Arnaud, J. D.; Hingant, E.; Pujo-Menjouet, L.; Liautard, J. P. Dynamics of Polymerization Shed Light on the Mechanisms that Lead to Multiple Amyloid Structures of the Prion Protein. *Biochim. Biophys Acta* **2011**, *1814*, 1305–1317.
24. Reinhard, B. M.; Siu, M.; Agarwal, H.; Alivisatos, A. P.; Liphardt, J. Calibration of Dynamic Molecular Rulers Based on Plasmon Coupling between Gold Nanoparticles. *Nano Lett.* **2005**, *5*, 2246–52.
25. Fezoui, Y.; Hartley, D. M.; Harper, J. D.; Khurana, R.; Walsh, D. M.; Condron, M. M.; Selkoe, D. J.; Lansbury, P. T.; Fink, A. L.; Teplow, D. B. An Improved Method of Preparing the Amyloid Beta-Protein for Fibrillogenesis and Neurotoxicity Experiments. *Amyloid* **2000**, *7*, 166–178.
26. Stine, W. B.; Dahlgren, K. N.; Krafft, G. A.; LaDu, M. J. *In Vitro* Characterization of Conditions for Amyloid-Beta Peptide Oligomerization and Fibrillogenesis. *J. Biol. Chem.* **2003**, *278*, 11612–11622.
27. Lomakin, A.; Teplow, D. B.; Kirschner, D. A.; Benedek, G. B. Kinetic Theory of Fibrillogenesis of Amyloid Beta-Protein. *Proc. Natl. Acad. Sci. U.S.A.* **1997**, *94*, 7942–7947.
28. Lomakin, A.; Chung, D. S.; Benedek, G. B.; Kirschner, D. A.; Teplow, D. B. On the Nucleation and Growth of Amyloid Beta-Protein Fibrils: Detection of Nuclei and Quantitation of Rate Constants. *Proc. Natl. Acad. Sci. U.S.A.* **1996**, *93*, 1125–1129.
29. Jarvet, J.; Damberg, P.; Bodell, K.; Eriksson, L. E. G.; Graslund, A. Reversible Random Coil to Beta-Sheet Transition and the Early Stage of Aggregation of the A Beta(12−28) Fragment from the Alzheimer Peptide. *J. Am. Chem. Soc.* **2000**, *122*, 4261–4268.
30. Yamaguchi, K.; Takahashi, S.; Kawai, T.; Naiki, H.; Goto, Y. Seeding-Dependent Propagation and Maturation of Amyloid Fibril Conformation. *J. Mol. Biol.* **2005**, *352*, 952–960.
31. Linse, S.; Cabaleiro-Lago, C.; Xue, W. F.; Lynch, I.; Lindman, S.; Thulin, E.; Radford, S. E.; Dawson, K. A. Nucleation of Protein Fibrillation by Nanoparticles. *Proc. Natl. Acad. Sci. U.S.A.* **2007**, *104*, 8691–8696.
32. Auer, S.; Trovato, A.; Vendruscolo, M. A Condensation-Ordering Mechanism in Nanoparticle-Catalyzed Peptide Aggregation. *PLoS Comput. Biol.* **2009**, *5*, e1000458.
33. Ni, C. L.; Shi, H. P.; Yu, H. M.; Chang, Y. C.; Chen, Y. R. Folding Stability of Amyloid-Beta 40 Monomer is an Important Determinant of the Nucleation Kinetics in Fibrillization. *FASEB J.* **2011**, *25*, 1390–1401.
34. Choi, I.; Huh, Y. S.; Erickson, D. Ultra-Sensitive, Label-Free Probing of the Conformational Characteristics of Amyloid Beta Aggregates with a SERS Active Nanofluidic Device. *Microfluid. Nanofluid.* **2012**, *12*, 663–669.
35. Stanyon, H. F.; Viles, J. H. Human Serum Albumin can Regulate Amyloid-Beta Peptide Fiber Growth in the Brain Interstitium Implications for Alzheimer Disease. *J. Biol. Chem.* **2012**, *287*, 28163–28168.
36. Biere, A. L.; Ostaszewski, B.; Stimson, E. R.; Hyman, B. T.; Maggio, J. E.; Selkoe, D. J. Amyloid Beta-Peptide is Transported on Lipoproteins and Albumin in Human Plasma. *J. Biol. Chem.* **1996**, *271*, 32916–32922.
37. Solomon, B.; Koppel, R.; Hanan, E.; Katzav, T. Monoclonal Antibodies Inhibit *In Vitro* Fibrillar Aggregation of the

Alzheimer Beta-Amyloid Peptide. *Proc. Natl. Acad. Sci. U.S.A.* **1996**, *93*, 452–455.
38. McLaurin, J.; Cecal, R.; Kierstead, M. E.; Tian, X.; Phinney, A. L.; Manea, M.; French, J. E.; Lambermon, M. H. L.; Darabie, A. A.; Brown, M. E.; *et al.* Therapeutically Effective Antibodies Against Amyloid-Beta Peptide Target Amyloid-Beta Residues 4−10 and Inhibit Cytotoxicity and Fibrillogenesis. *Nat. Med.* **2002**, *8*, 1263–1269.
39. Ladiwala, A. R.; Bhattacharya, M.; Perchiacca, J. M.; Cao, P.; Raleigh, D. P.; Abedini, A.; Schmidt, A. M.; Varkey, J.; Langen, R.; Tessier, P. M. Rational Design of Potent Domain Antibody Inhibitors of Amyloid Fibril Assembly. *Proc. Natl. Acad. Sci. U.S.A.* **2012**, *109*, 19965–19970.
40. Kuo, Y. M.; Kokjohn, T. A.; Kalback, W.; Luehrs, D.; Galasko, D. R.; Chevallier, N.; Koo, E. H.; Emmerling, M. R.; Roher, A. E. Amyloid-Beta Peptides Interact with Plasma Proteins and Erythrocytes: Implications for Their Quantitation in Plasma. *Biochem. Biophys. Res. Commun.* **2000**, *268*, 750–756.